Dynamics of water coning

Jonn-Erik Farmen,[1] Geri Wagner,[1,*] Unni Oxaal,[1,2] Paul Meakin,[1] Jens Feder,[1] and Torstein Jøssang[1]
[1]*Department of Physics, University of Oslo, P.O. Box 1048, Blindern, N-0316 Oslo, Norway*
[2]*Department of Agricultural Engineering, Agricultural University of Norway, P.O. Box 5065, N-1432 Ås, Norway*
(Received 14 September 1998; revised manuscript received 1 June 1999)

Water beneath a layer of oil in a producing reservoir may rise and form a bell-shaped cone in the vicinity of the well. We discuss how the dynamics of cone formation in two dimensions depends on the gravitational contrast, the interfacial tension, and the flow rate of oil. For a constant flow rate below a critical rate Q_c, stable cones are formed. At rates above Q_c, two dynamical regimes are expected. These are slow initial formation and fast breakthrough to the well. Quasi-two-dimensional transparent porous models were used to perform cone formation experiments. Effective acceleration due to gravity was systematically varied. The experiments were simulated using a stochastic model based on invasion percolation in which capillary forces were explicitly taken into account. We find agreement between experiments and simulations, and consistency with the theoretical predictions. [S1063-651X(99)07609-6]

PACS number(s): 47.55.Mh, 47.55.Kf, 91.65.−n

I. INTRODUCTION

In oil reservoirs, a layer of water often lies beneath a layer of oil. As the oil is produced from a well in the oil layer, the oil-water interface is deformed into a characteristic bell-like shape, the *water cone* [see Fig. 1(a)]. The deformation is driven by the viscous pressure gradient in the vicinity of the well, and counterbalanced by gravity forces due to the density difference between the rising water and the oil. If the flow rate of oil is lower than a critical flow rate Q_c, equilibrium is reached and a static water cone forms. In the field, coning is highly undesirable, as it limits production and reduces recovery of reserves. Unfortunately, the technology for abatement of coning is still at an early stage [1].

For the physicist, water coning presents an interesting moving-boundary problem. The pressure distribution in the reservoir is determined by viscous and hydrostatic contributions. During the coning process the boundary conditions at the oil-water interface change. Depending on the flow rate, cone propagation either comes to a halt (a stable cone is formed) or continues up to the well (the cone growth process is unstable). In addition, the properties of the reservoir influence cone formation. For instance, if the water is nonwetting with respect to the oil, then the capillary pressure across the oil-water interface opposes cone propagation.

A number of workers have attempted to characterize breakthrough conditions and the shape of stable cones, in two- and three-dimensional reservoirs [2–10]. (Two-dimensional geometries are used to study coning below horizontal wells, where oil is flowing to a line sink.) On the experimental side, Khan [11], Mungan [12], and Rajan and Luhning [13] built three-dimensional scaled reservoir models and studied the shape of stable cones and breakthrough rates under various circumstances. Schols [14] directly observed water coning in a Hele-Shaw cell and presented an empirical formula to predict critical flow rates.

However, equally important questions concern the *dynamics* of cone formation. The issue is relevant for petroleum engineering because water-free oil can be produced at a supercritical rate during the cone buildup time. The advantage of a higher flow rate must then be balanced against the disadvantage of earlier water breakthrough. The dynamics of water coning is difficult to study in the field, due to the considerable effort required to map the cone shape, and the lack of detailed knowledge of the reservoir properties. Sobocinski and Cornelius [15] were among the first to discuss dynamics, and observed cone formation under the well in a wedge-shaped reservoir model. Breakthrough times were calculated numerically by Ozkan and Raghaven [16] and Papatzacos *et al.* [17].

In this paper we study the dynamics of water coning in two-dimensional porous media. In Sec. II, experiments are presented in which a water cone formed below a well in a

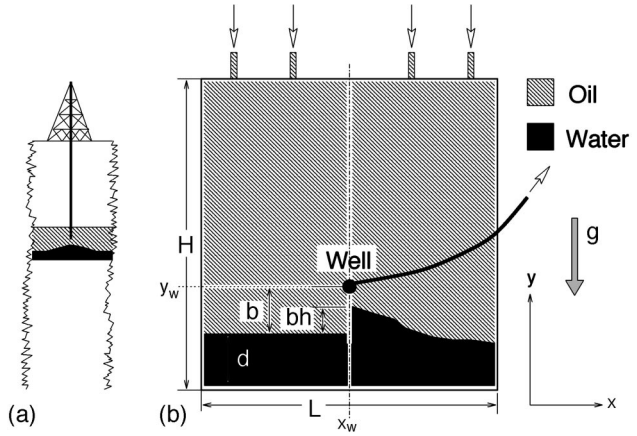

FIG. 1. (a) illustrates the formation of a water cone (black) in a region saturated with oil (shaded) in the vicinity of a well. (b) is a schematic drawing of a two-dimensional reservoir model at the beginning of (left-hand section) and during water coning (right-hand section). Oil is flowing in at the top rim and pumped out through the well in the center of the model. The direction of gravity g is indicated.

*Present address: School of Astronomy and Physics, R. and B. Sackler Faculty of Exact Sciences, Tel Aviv University, Israel.

layer saturated with oil. Included is a preliminary presentation of an experiment in which an additional gas phase was superposed on the oil layer. Using the experiments as a reference, a stochastic simulation model based on the invasion percolation model was constructed. The simulations are described in Sec. III. Some theoretical predictions for the scaling behavior of cone formation are derived in Sec. IV, and experimental and simulation results are presented in Sec. V. We discuss our results and conclude in Sec. VI.

II. EXPERIMENTS

The quasi-two-dimensional porous models used in the experiments consisted of a monolayer of 1 mm glass beads sandwiched between two 25 mm thick parallel polymethylmethacrylate (PMMA) plates. These models measured $L = 41$ cm$\times H = 44$ cm in size and had a porosity of $\varphi = 0.54$ and a permeability of $k = 6\times 10^{-6}$ cm^2. The width of the water layer was $d = 6$ cm, and the distance from the initial oil-water interface to the well was $b = 8$ cm. Model construction elements were identical to those described in Ref. [18]. A hole of 5 mm diameter in the center of the model represented an oil well. Ducts at the lower and upper rim of the model were used to fill the model with the fluids prior to starting the experiments.

For each experiment, a new model was used. During the filling process, the model was tilted to a vertical position, and a water-glycerol mixture (75 wt% water) representing water was slowly injected through ducts at the lower end of the model. When the lower portion of the model was completely saturated with the water-glycerol mixture, olive oil was injected through ducts at the upper end of the model. This procedure was chosen in order to achieve a homogeneous distribution of fluids in the various portions of the model. Good control of the initial conditions in an experiment was essential, as the wetting properties of the model were history dependent. In a region that was intially saturated by oil, the invading water-glycerol mixture was nonwetting and water coning was opposed by capillary forces. On the other hand, the water-glycerol mixture was the wetting fluid for regions that were initially saturated by the water-glycerol mixture. Oil displacing the water-glycerol mixture in those regions was nonwetting, and again water coning was opposed by capillary forces. The wetting angle θ was close to 90° [19], and no significant hysteresis was observed.

Two-layer reservoirs, consisting of an oil layer above a water layer, were modeled by saturating the upper portion of the model with olive oil. Three-phase experiments were also conducted. In these experiments, an additional gas layer above the oil layer was modeled by saturating only the center portion of the model with oil. A dyed citrus-oil–paraffin mixture representing gas was injected into the upper portion. The fluids were chosen to match the ratios of density, viscosity, and interfacial tension of the reservoir fluids in the Gullfaks formation in the North Sea as closely as possible. Table I lists relevant properties of the reservoir fluids and the model fluids.

To begin an experiment, the model was tilted to a suitable angle of inclination α and the ducts at the lower end of the model were closed. A peristatic pump extracted the oil from the model through the well at the center of the model, at a constant rate Q. Pump rates varied from 0.3 ml/min to 10 ml/min. In the two-layer reservoir experiments, an outer oil reservoir was connected to the model through ducts at the upper rim, and the amount of oil in the model remained constant. In the three-layer reservoir experiments, a similar reservoir containing citrus-oil–paraffin mixture was used. In this case, the volume of olive oil in the model decreased during an experiment while the volume of citrus-oil–paraffin mixture increased. In both types of experiment, the amount of the water-glycerol mixture in the model remained constant.

TABLE I. Table of fluid properties in the Gullfaks reservoir, and used in the model at 20 °C, including viscosity μ, density ρ, and interfacial tension with respect to oil σ. Olive oil representing oil in the experiment and citrus-oil–paraffin mixture representing gas were miscible. Olive oil and the water-glycerol mixture representing water were immiscible.

Fluid		ρ (kg/m^3)		μ (cP)		σ (N/m)	
Res.	Expt.	Res.	Expt.	Res.	Expt.	Res.	Expt.
Gas	Citrus-oil–paraffin	280	864	3	4		
Oil	Olive oil	645	911	46	65	0.001	0
Water	Water–glycerol	1000	1199	25	27	0.02	0.036

Figure 2 shows the formation of a water cone in a two-layer model inclined at $\alpha = 18°$ from the horizontal. The flow rate was kept at a constant value of $Q = 4.4$ ml/min. The water-glycerol mixture–olive-oil interface evolved from a flat front to a bell-shaped curve with a cusp. Breakthrough occurred after approximately 10 min.

Capillary forces can affect the coning process significantly. In Fig. 3, a cone front observed in a vertical model

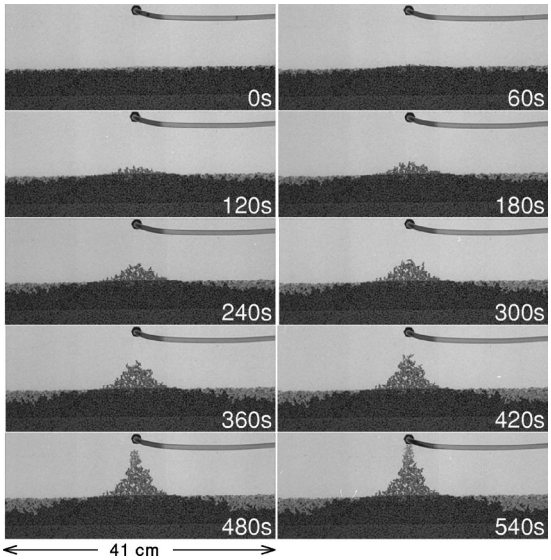

FIG. 2. Water coning at constant flow rate of $Q = 4.4$ ml/min in a two-layer reservoir model. The model was saturated with a water-glycerol mixture (dark) in the lower portion, and with olive oil (light) in the center and upper portion. Time is indicated in seconds. Inclination 18° from the horizontal.

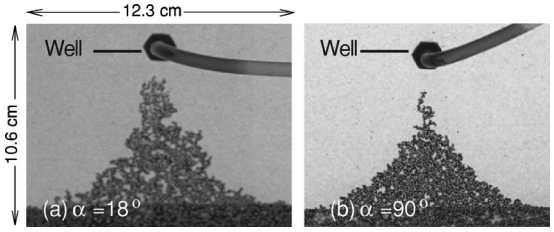

FIG. 3. Water cone tips immediately before breakthrough in two-layer models at $Q=4.4$ ml/min and inclinations of $\alpha=18°$ and 90°, respectively.

($\alpha=90°$) is compared with a front observed in an inclination of 18°. (a) shows a detail of the sequence shown in Fig. 2. For low gravitational contrasts $\Delta\rho g$, pinning of the propagating front occurs. The resulting front is rough, and large regions of oil became trapped in the cone. In the vertical model, gravity forces are stronger by a factor of 3 and are comparable to capillary forces only on a length scale of the order of a typical pore size a. The cone is smooth on length scales larger than a, and trapping of oil is rare.

Figure 4 shows the formation of a cone in a three-layer model, at a constant flow rate of $Q=8.8$ ml/min. In the upper section of the model, the gas intruded in the form of viscous fingers, directed towards the well. Gas fingers reached the well after about 5 min, and oil production declined. At this stage, a pronounced, apparently static, water cone had formed below the well. The experiment was terminated after ten additional minutes during which no further cone propagation was observed.

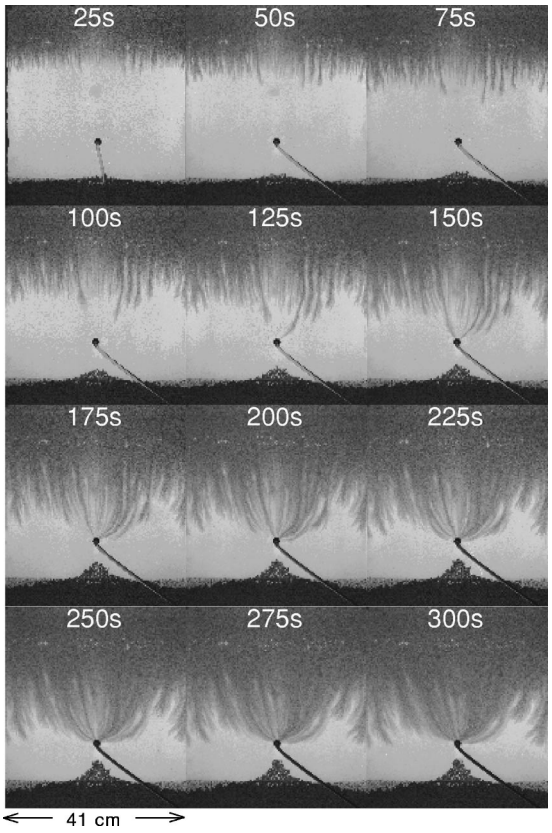

FIG. 4. Water coning at constant flow rate in a three-layer model. The model was saturated with water-glycerol mixture (dark) in the lower portion, with olive oil (light) in the center portion, and with citrus-oil–paraffin mixture (dark gray) in the upper portion. Time is indicated in seconds.

III. SIMULATIONS

Water coning in two-layer reservoirs was simulated using a stochastic simulation model of the invasion percolation type [20,21] in which viscous forces are taken into account and fluid migration is possible. The pores in a porous model were represented by a square lattice of sites. The sites were labeled to represent pores occupied by either olive oil or a water-glycerol mixture. At the beginning of each simulation, a radius a_i was assigned to the pore represented by the ith site. The distribution of the radii $\{a\}$ approximated the pore neck size distribution identified in a digitized image of an experimental model. The distribution increased approximately linearly up to a peak at $a\approx0.1$ mm. For $a>0.1$ mm the distribution decreased approximately exponentially, ranging up to approximately $a=0.5$ mm.

In the continuum approximation, the potential field Φ of an incompressible fluid in quasistationary flow satisfies the Poisson equation $\nabla^2\Phi=T$, where T represents the sources and sinks. In the simulation, the fluid potential due to oil production was found by solving the Poisson equation on all sites of the lattice that were occupied with oil, using a relaxation method [22]. The boundary conditions used were $\Phi=0$ at the top row representing the reservoir of olive oil (inlet), and $\mathbf{n}\cdot\boldsymbol{\nabla}\Phi=0$ at all other boundaries (remaining lattice boundaries and interfaces with regions filled with the water-glycerol mixture), where $\mathbf{n}$ is a unit vector normal to the boundary or interface. At one site representing the well, a finite source term $T=Q\mu\delta(\mathbf{r}-\mathbf{r}_w)/(kD)$ was used, where Q is the flow rate or production rate, μ the viscosity of the oil, δ the Dirac delta function, $\mathbf{r}_w=(x_w,y_w)$ the location of the well, k the permeability of the medium, and D the thickness of the model. At all other sites, T was set to 0. To include the effects of gravity, a hydrostatic pressure contribution $P_g=\rho_o gh$ was added, where h is the distance to the upper lattice boundary.

The viscosity of the water-glycerol mixture was neglected so that no viscous forces were present on sites occupied by water-glycerol ($\Phi=0$). Pressure in the water-glycerol mixture region was calculated relative to the reference pressure $P_{\mathrm{ref}}=\Phi+P_g$ at the lowest oil-occupied site on the lattice. For the ith water-glycerol mixture site, pressure was then given by $P=P_{\mathrm{ref}}+\rho_W g\Delta h_i$, where Δh_i is the height difference between the ith site and the reference site.

The capillary pressure P_c across a pore containing the oil-water interface was given by Young's law, $P_c=\sigma(2D^{-1}+2a^{-1})$, where D is the distance separating the PMMA walls of the porous models, and a the diameter of the pore [see Fig. 5(a)].

At the start of a simulation, all sites in the lower portion of the lattice were labeled to represent the water-glycerol mixture. The remaining sites on the lattice represented oil. The simulations proceeded in steps in which water-glycerol mixture invaded a site previously occupied by oil, and simultaneously abandoned a site [see Fig. 5(b)]. Only sites at the interface between the two phases could be invaded or abandoned. At each stage, steps were chosen randomly among a

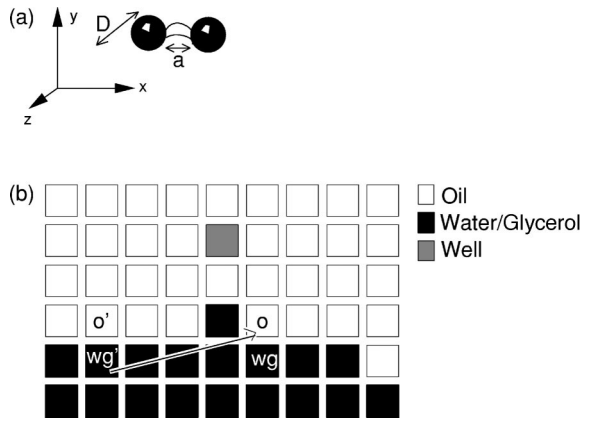

FIG. 5. Illustration of the simulation model. (a) Capillary pressures in pores were calculated according to Young's law. (b) The porous model was represented by a square lattice of sites. In each simulation step, water-glycerol mixture propagated into an oil-filled pore (o), and oil propagated into a water-glycerol mixture–filled pore (wg'). The step was possible if the total pressure balance $\Delta P_{wg\to o}-\Delta P_{o'\to wg'}$ was positive.

set of possible steps. This set included all steps with a positive pressure balance

$$\Delta P=\Delta P_{wg\to o}-P_c^{(o)}-\Delta P_{o'\to wg'}-P_c^{(wg')} \tag{1}$$

in which the condition

$$P^{(o)}<P^{(wg')} \tag{2}$$

was fulfilled. In Eq. (1), $\Delta P_{wg\to o}$ is the pressure difference across the interface at the point where propagation of the water-glycerol mixture into the oil-filled region occurs. $\Delta P_{o'\to wg'}$ is the corresponding pressure difference at the point where the water-glycerol mixture retreats. $P_c^{(o)}$ and $P_c^{(wg')}$ denote the capillary pressures that must be overcome in the step. The balance was typically positive for steps in which the water-glycerol mixture propagated upwards in the vicinity of the well and retreated at the boundaries of the lattice. The condition Eq. (2) eliminated unphysical steps and required that the pressure at the oil-filled pore that became invaded with the water-glycerol mixture be less than the pressure at the pore from which the water-glycerol mixture withdrew.

Among all possible steps, the ith step was selected randomly with the probability p_i proportional to ΔP_i. In a sense, this rule is an extrapolation of Darcy's law to the pore level, for the case of equal permeability at all pores. (An alternative rule in the spirit of the invasion percolation model is to select, at each stage, the step providing the largest pressure difference ΔP. That rule led to propagation only below the well and thus to very poor representations of the cone formation process.) To establish a time scale, the time was incremented by $\Delta t=1/N$ during each step, where N is the number of possible steps at each stage.

After each step, the viscous and hydrostatic pressure fields were recalculated, and the boundary conditions were updated to account for the the changing oil-water interface. Then a new set of acceptable steps was compiled, and the next step was executed. The simulations were terminated when no step with positive pressure balance was possible or when the water-glycerol mixture reached the well site.

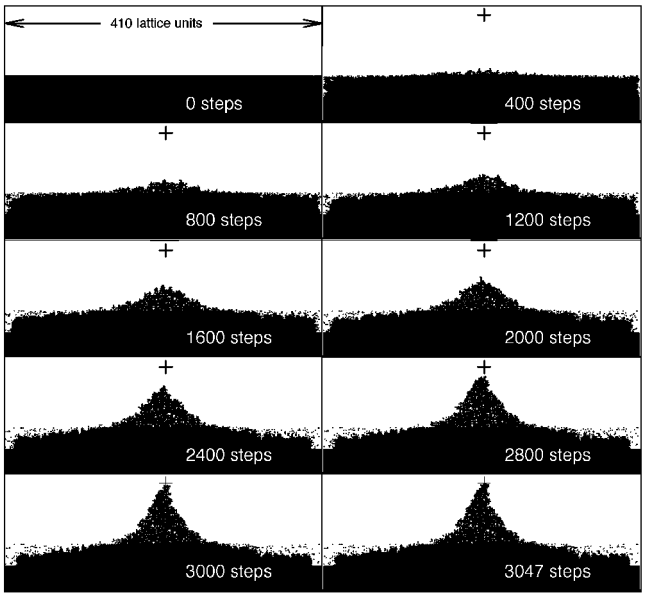

FIG. 6. Structures observed at various stages in a simulation of water coning at constant flow rate $Q=4.4$ ml/min and an inclination of $\alpha=18°$. The water-glycerol mixture is shown in black and olive oil is shown in white. The simulation was terminated when the cone had reached the well, after 3047 steps. Only part of the 440×410 lattice is shown. The figure should be compared with Fig. 2; the same parameters were used in experiment and simulation.

To account for low fluid compressibilities, a trapping rule [21] was used to prevent water-glycerol mixture from invading oil-filled pores that were not connected to the well by a path of nearest-neighbor steps between oil-filled pores. Withdrawal of the water-glycerol mixture often led to fragmentation of the water-glycerol cluster, and occasionally ''untrapping'' of trapped oil regions.

The simulation model was calibrated to enable quantitative comparison with experiments. Production rate Q was determined directly by measuring the fluid potential gradient $\nabla\Phi$ at the inlet boundary. Q was given by $Q=A(k/\mu)\nabla\Phi$, where $A=4.1\times10^{-4}$ m^2 is the cross section of an experimental model. Values for k, μ, σ, ρ_o, and ρ_{wg} measured for the fluids used in the experimental system were used. Pore radii a varied between 0.01 mm and 0.5 mm, and a value of $D=1$ mm was used to assign capillary pressures. The dimensions of the experimental model were retained. To simulate experiments on inclined models, an effective acceleration due to gravity of $g=g_0\sin\alpha$ was used, with $g_0=9.81$ m/s^2.

Lattices of 440×410 sites were used in an attempt to model the experiments as closely as possible. Due to the need to repeatedly solve the Poisson equation, the simulations required a large amount of computer time, ranging from days to a few weeks for the longest runs. Figure 6 shows several stages during a simulation, using a flow rate of $Q=4.4$ ml/min and $\alpha=18°$. Important features of the simulated structures are in qualitative agreement with the experiments. These include the gradual formation of a rough interface, the withdrawal and fragmentation of the water-glycerol mixture in boundary regions, the complex disorderly cone

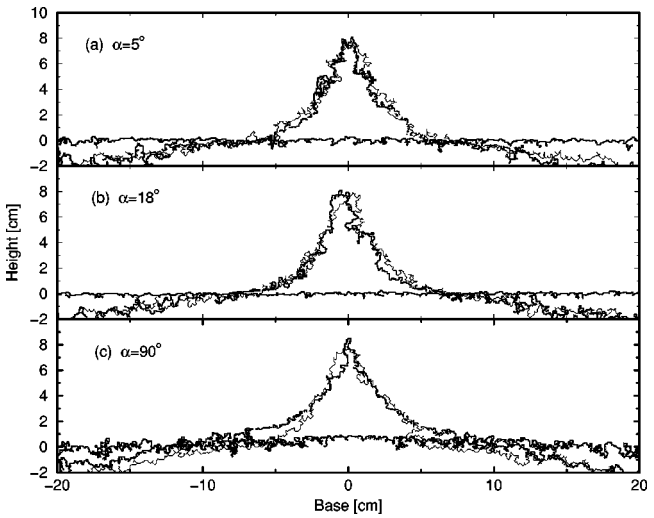

FIG. 7. Cone fronts (bold lines) observed at initial and near-final stages, respectively, in a two-layer reservoir model. The flow rate was $Q=4.4$ ml/min. (a), (b), and (c) show experiments at inclinations of 5°, 18°, and 90° from the horizontal, respectively. The fronts observed at the final stages of the simulations (regular lines), using parameters matching the experiments, are also shown.

profile, and the trapping of oil in the propagating cone.

Figure 7 shows direct comparisons of cone fronts observed in experiments and simulations, at a constant flow rate of $Q=4.4$ ml/min and varying effective acceleration due to gravity (or cell inclination). The simulated cones are in fair agreement with the experimental structures, although significant deviations are apparent at $\alpha=90°$. Moreover, the differences in front roughness resulting from varying α appear less pronounced in the simulations.

IV. SIMPLE THEORY OF CONING

In this section we derive a continuum analog to Eq. (1), expressing the sum of pressure differences across the interface at the tip of the cone and far from the well. We set the well at the center of the coordinate system, and define the cone height bh in terms of the initial distance b from the initial oil-water interface to the well [see Fig. 1(b)], and the dimensionless cone height $0<h<1$.

In the Muskat approximation [2,4,6,7,23], it is assumed that the potential Φ in the oil layer is not affected by the presence of the rising water cone. In an infinite two-dimensional reservoir, this implies $\Phi(r)\sim Q\ln(r/r_0)$ at all stages for the solution of the Poisson equation, where r is the distance to the well, and r_0 is a length scale characterizing the problem. Let us ignore finite-size corrections, and let us assume, as in the simulation model, that the viscosity of the water is much smaller than that of the oil. In that case, $\Phi=0$ in the water layer because the viscous forces are not transmitted across into the oil-water interface.

Consider now the pressure differences ΔP across the interface, ignoring capillary forces for the moment. Far from the well, $\Delta P\approx 0$ because the influence of the well on the potential is small. At the tip of the cone [see Fig. 1(b)], the pressure in the oil layer is $P_{\rm tip}^{(o)}=AQ\ln[(1-h)b/r_0]+\rho_o gb(1-h)+P_0$. Here, the first term represents the difference $\Delta\Phi_{\rm tip}$ in fluid potential at the cone tip, and $A=\mu/(2\pi kD)$ is a prefactor. P_0 is a constant, and ρ_o and g denote the density of the oil and the acceleration due to gravity, respectively. In the water layer at the cone tip, the pressure is given by hydrostatic contributions only; $P_{\rm tip}^{(w)}=\rho_o gb(1-h)-\Delta\rho gbh+P_0$, where $\Delta\rho=\rho_w-\rho_o$ is the difference in density between water and oil. Cone propagation is driven by the sum $\Delta P_{\rm tot}$ of pressure differences across the interface at the tip and far from the well,

$$\Delta P_{\rm tot}=AQ\ln\left[\frac{r_0}{b(1-h)}\right]-\Delta\rho gbh-2P_c. \qquad (3)$$

The last term in Eq. (3) represents the average capillary pressures which we take to be negative across both the tip section and the boundary sections of the interface (opposing cone propagation).

Equation (3) is the required continuum analog and can now be used to discuss qualitatively the dynamics of water coning. For very low Q, $\Delta P_{\rm tot}$ is negative at $h=0$ due to the capillary pressure, and no cone can be formed. For intermediate Q, cone propagation is possible up to a critical height $h_c(Q)$, where $\Delta P_{\rm tot}$ again becomes negative, due to the increasing hydrostatic term. For high $Q>Q_c$, $\Delta P_{\rm tot}$ is positive for all h and breakthrough occurs. If the gravitational contrast $\Delta\rho g$ is increased, Q_c is shifted and breakthrough requires even higher flow rates.

The dimensionless cone height is a function of time, $h=h(t)$. To estimate the cone propagation velocity, we assume that the velocity $v_{\rm tip}$ of tip advancement is directly proportional to the pressure difference $\Delta P_{\rm tot}$ that drives propagation at each stage, $v_{\rm tip}\sim\Delta P_{\rm tot}$. For small h, $v_{\rm tip}$ depends, to first order, linearly on h. At $\ln(1-h)\approx -1$, or $h=(e-1)/e\approx 0.63$, $v_{\rm tip}(h)$ undergoes a transition from approximately linear dependence to exponential increase. This transition is due to the logarithmic term in Eq. (3) and occurs independently of the values of $Q>Q_c$ and $\Delta\rho g$.

The breakthrough time $\tau(Q;\Delta\rho g;P_c)$ is found by integrating $1/v_{\rm tip}$ over h. This must be done numerically. Keeping $\Delta\rho g$ and P_c constant and varying Q, breakthrough time for flow rates above the critical one is well described by the form $\tau(Q)\sim 1/(Q-Q_c)^{0.9}$. Keeping Q and P_c constant and varying $\Delta\rho g$, a reasonable approximation for τ is $\tau(\Delta\rho g)\sim 1/(\Delta\rho g_c-\Delta\rho g)^{0.6}$, where $\Delta\rho g_c$ is the critical gravitational contrast above which breakthrough is not possible for a given rate Q. Finally, keeping Q and $\Delta\rho g$ constant and varying the capillary pressure P_c or the interfacial tension σ, $\tau(\sigma)\sim 1/(\sigma_c-\sigma)^{0.6}$ is found, where σ is the maximum interfacial tension allowing for coning.

V. RESULTS

Figure 8 shows a plot of the normalized cone height h as a function of time, measured in three experiments and simulations at the same constant flow rate Q, for several values of α. In the simulations, time is given in arbitrary units since fluid flow is modeled in discrete steps only. As expected, breakthrough time increased as the effective gravity forces increased. In all cases, the propagation velocity, corresponding to the slope of the curve, increased when the relative height h surpassed a value of about 2/3 of the maximum height $h=1$.

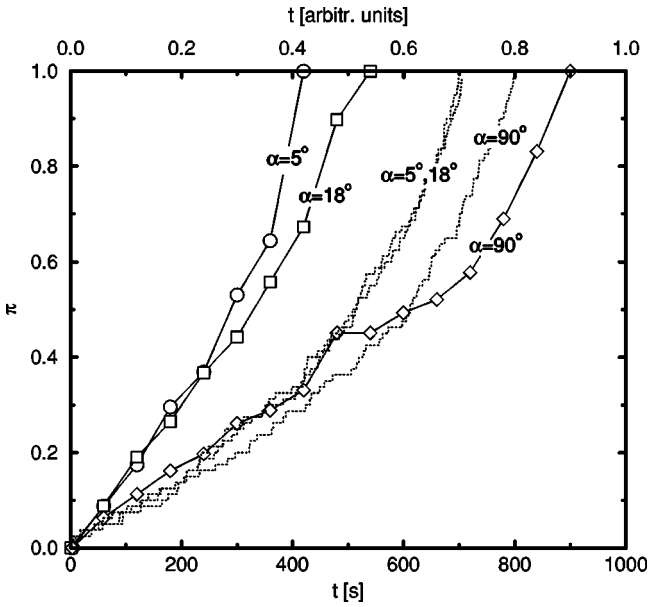

FIG. 8. Plot of the normalized cone height h as a function of time, measured in two-phase experiments (symbols) and simulations (dotted lines) at $Q=4.4$ ml/min and various inclinations α. For the simulations, time is given in arbitrary units (upper scale).

It is apparent that the effects of decreasing α are not well reproduced in the simulations; the change in propagation velocity is too small. The curves corresponding to $\alpha=5°$ and 18°, respectively, cannot easily be distinguished on the scale of the plot. At this point, however, the stochastic nature of both the experiments and the simulations must be stressed.

Statistical fluctuations can only be reduced by averaging over many realizations. To this end, simulations were performed on much smaller lattices of size 82×88 sites. On this scale, a simulation was completed within a few minutes. Figure 9(a) shows a plot of cone growth curves $h(t)$ similar to

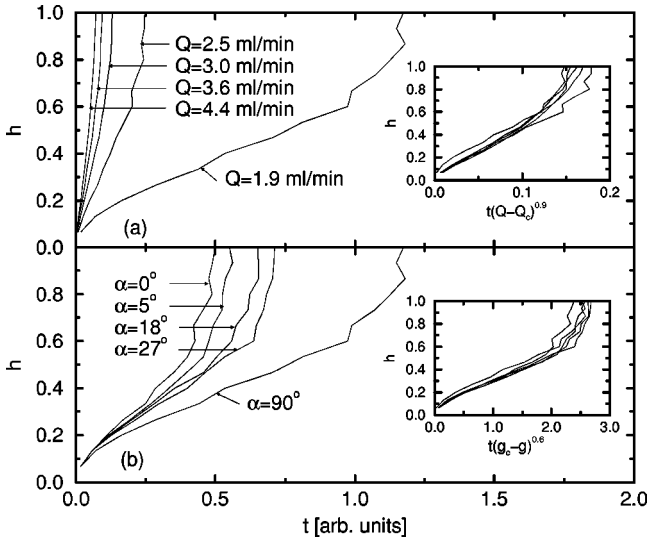

FIG. 9. Plot of the normalized cone heights h as a function of time, measured in simulations and averaged over several hundred realizations. (a) shows $h(t)$ for $\alpha=90°$ and various flow rates Q. (b) shows $h(t)$ for the constant rate $Q=1.9$ ml/min and various inclinations α. The insets show attempts to collapse the data on curves, using $Q_c=1.8$ ml/min and $g_c=13.5$ m/s^2.

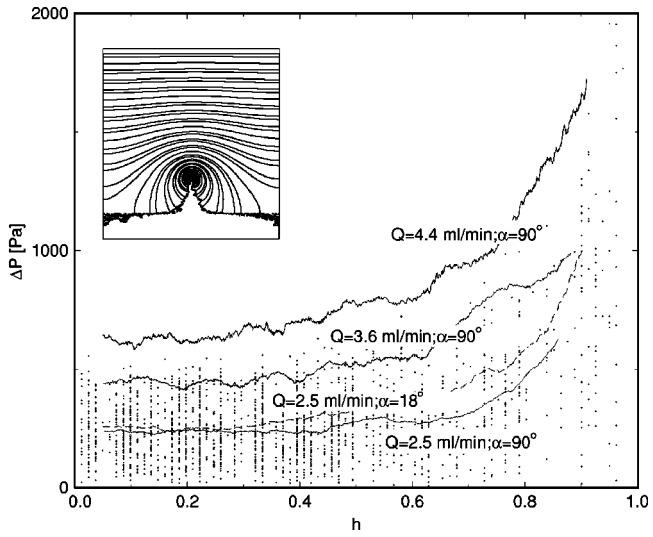

FIG. 10. Running averages of ΔP measured in simulations for various values of Q and $\alpha=90°$ (solid lines) and for $Q=2.5$ ml/min and $\alpha=18°$ (dashed line). Also shown is the complete sequence of measurements for $Q=2.5$ ml/min and $\alpha=90°$ (dots). The inset shows contours of the fluid potential Φ measured at the final stage in a simulation, using $Q=2.5$ ml/min and $\alpha=90°$.

the ones shown in Fig. 8, representing averages of several hundred runs. In these simulations the effective acceleration due to gravity, g, was set to 9.81 m/s^2 ($\alpha=90°$). At the lowest rate shown, $Q=1.9$ ml/min, breakthrough time increased markedly, and breakthrough occurred only in 60% of the runs. (In the remaining 40% of the runs, a stable cone was formed.) (b) shows cone growth curves measured at a constant low pump rate $Q=1.9$ ml/min and several values for the acceleration due to gravity. The insets show the results of the attempts to collapse the data on single curves, based on the empirical fits obtained from integrating the expression $1/\Delta P(h)$. In both parts, the data collapses are quite good, considering that Eq. (3) is based on gross simplifications. Only one of the simplifications was explicitly built into the simulation model, namely, $\Phi=0$ in the water layer.

Pressures can be measured readily in the simulations, and the validity of Eq. (3) can be checked directly. Figure 10 shows a plot of ΔP as a function of the normalized cone height h, measured during simulation runs (using the larger lattice). $\Delta P(h)$ is a multivalued function since not every step in the simulation leads to a cone height increase. Also, the values of ΔP vary randomly since they depend on the random capillary pressures and on the sequence of propagation steps.

Running averages of ΔP confirm the simple picture given in connection with Eq. (3). For a given combination of Q and α, ΔP varied approximately linearly with h for $h<0.6$. At very low production rates ($Q=1.7$ ml/min; not shown in the figure), breakthrough was barely possible, and ΔP decreased linearly with h for small h. At higher rates, ΔP increased monotonically with h. For large h, ΔP increased steeply in all cases. As in Fig. 8, a transition to fast cone propagation can be observed at $h\approx0.65$.

In quantitative terms, however, the agreement with Eq. (3) is poor. The reasons for that are threefold. First, the po-

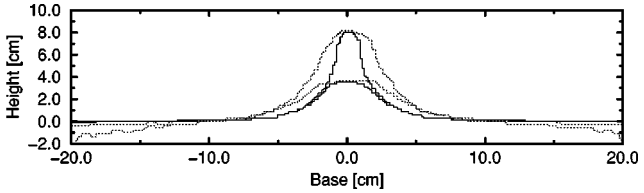

FIG. 11. Cone fronts at $h=0.5$ and $h=1$ found by averaging over several hundred simulations on small lattices, using $\alpha=90°$ and $Q=1.9$ (solid lines) and 4.4 (dotted lines) ml/min, respectively.

tential field $\Phi(\mathbf{r})$ in the oil layer must meet the boundary conditions imposed by the geometry of the experimental model, which leads to a flattening of the potential close to the boundaries of the oil layer. The discrepancy to the logarithmic solution, on which Eq. (3) is based, is most pronounced for small h. Secondly, as Q is increased, the cone broadens and an increasing number of simulation steps represent flow of water to the slopes of the cone, as opposed to flow of water to the tip of the cone. This effect reduces the running average of ΔP so that a direct comparison with ΔP_{tot} is not possible. Thirdly, as the cone rises, the potential field starts to deviate from its original form, in contradiction to the Muskat approximation underlying Eq. (3). These three effects conspire to lower the average driving contribution $\Delta\Phi$ to Eq. (3), and leave the opposing contributions unchanged. The factor by which $\Delta\Phi(h)$ is reduced depends weakly on the flow rate Q but is roughly equal for all cone heights h. For this reason, the averages shown in Fig. 10 are still reasonably well described by the form given in Eq. (3), provided that the prefactor A of the logarithmic term be changed adequately. Moreover, the scaling predictions for breakthrough times hold, as shown in Fig. 9.

The sequence of simulations at small scales may also be used to study the cone shape at various stages during the formation, by averaging the individual shapes. A convenient method is to identify all lattice sites that become invaded in more than 50% of the realizations, and use them to represent the cone. The resulting structure is free of random fluctuations while the effects of capillary forces still are taken fully into account. The result is shown in Fig. 11, for two different flow rates Q. As the viscous forces increase (or the gravity forces decrease), a large amount of water is redistributed and the cones become more massive. It is interesting that at the limiting flow rate Q_c the cone does *not* degenerate into a vertical line, since the ratio of driving forces and opposing forces is not constant during cone formation.

VI. DISCUSSION

The importance of capillary effects in the experiments is apparent. Random capillary forces can pin the propagating oil-water interface, leading to a rough front. A dimensionless capillary number $\mathrm{Ca}_{\mathrm{tip}}$, describing the advancement of the cone tip, can be defined by $\mathrm{Ca}_{\mathrm{tip}}=\mu_w v_{\mathrm{tip}}/\sigma$. During most of the formation time, v_{tip} was of the order of 10^{-4} m/s. Inserting the values μ_w and σ for the viscosity of the water-glycerol mixture and the interfacial tension, $\mathrm{Ca}_{\mathrm{tip}}\approx 10^{-4}$ is obtained. Displacement processes of oil by water in this regime are known to be dominated by capillary forces [24].

Capillary forces were explicitly taken into account in the simulations. The simulations combine a discrete lattice model of the porous model with a continuum description of the pressure field. Similar approaches have provided good results in the context of slow fluid-fluid displacements in uniform gravity fields [25–29] and, more recently, in viscous pressure fields [30]. Additional successful approaches of this sort include diffusion-limited-aggregation-like models of fast fluid-fluid displacements [31–33]. In the present case, a surprisingly realistic representation of the coning process in a two-layer scenario was obtained. However, discrete percolation-like models like the one used in this work do not provide intrinsic time scales. Since the primary object of this work was the study of dynamics, the time Δt that elapsed at each stage had to be defined *ad hoc*, as being inversely proportional to the number of possible moves. This definition is customarily chosen to represent processes that overlap in time, such as the simultaneous flow of water from various parts of the water layer into the rising cone.

Using this time scale, direct comparisons of cone growth curves $h(t)$ in experiments and in simulations showed only moderate agreement. These comparisons were based on single realizations and are significantly affected by random fluctuations. Yet it is apparent that the simulations did not reproduce the effect of decreasing relative magnitude of gravity forces correctly. This conclusion is also supported by Fig. 7. Possible reasons include an underestimate of the permeability of the experimental model, leading to a systematic underestimate of simulated flow rate. In this case, the ratio of gravity and capillary forces to viscous forces is too small, and variations of the former are masked by the dominant viscous forces.

Gravity opposes the tendency to form capillary fingers and smoothes the cone front, as shown in Figs. 3 and 7. On the scale of the experiments, the local roughness of the front could not be measured unambiguously. By analyzing the data shown in Fig. 7, the width of the front was found to decrease with increasing α, in both experiments and simulations, as expected. Here the width was quantified by measuring the standard deviation of a front from its running average, in a small interval defined by $0.4<h<0.6$. However, the quality of the data did not allow for quantitative statements.

The scale of the front roughness is given by the ratio of capillary forces to the remaining forces. The local front width ξ can be expected to vary continuously along the front since this ratio is small below the well and increases in boundary regions far from the well. In gravity-stabilized fluid-fluid displacement experiments (in the absence of viscous forces), it is well known that $\xi\sim|\mathrm{Bo}|^{-\nu/(\nu+1)}$, where the Bond number Bo is the ratio of gravity forces to capillary forces and ν is the percolation correlation exponent [25,27]. A similar relationship seems to hold for fluid-fluid displacement processes that are driven by weak viscous forces (in the absence of gravity), where the capillary number Ca replaces the Bond number Bo [30]. An analog scaling law for the front width in water coning may involve a combination of Bo and Ca. In practice, the capillary-induced roughening of the front will be small on the overall scale of the cone, which is given by the size of the reservoir (tens of meters in typical oil fields). Nevertheless, capillary forces should not be neglected even on the reservoir scale since they make a crucial contribution to the overall pressure balance that controls

cone propagation. For instance, heterogeneities in the reservoir can distort the cone shape significantly due to the combined effects of variations in capillary pressure and permeability. The scaling predictions for breakthrough times will break down altogether in that case. One way to investigate coning in such a scenario, next to detailed experimental studies, is to construct a computer model in which the pore radii associated to the sites reflect the spatial distribution of reservoir permeability. To model coning in a reservoir, rather than in a laboratory model, each site will represent a macroscopic rock section rather than a single pore.

In conclusion, we studied water cone formation in homogeneous two-dimensional porous models in experiments and simulations. Our simulations involve a combination of a percolationlike model with a continuous pressure field describing the viscous fluid flow. We presented a simple approach to understand the dynamics of the process, based on the Muskat approximation, and find that cone formation is characterized by a transition from slow to fast cone growth. Finally, we speculate on the dynamics of coning in three-dimensional systems. The potential field in the oil layer is then described by a function of the form $1/r$. No pronounced transition from slow to fast cone propagation, but a gradual increase in propagation velocity with increasing cone height, should be expected in that case.

ACKNOWLEDGMENTS

We gratefully acknowledge the financial support of The Research Council of Norway (NFR) and VISTA, a research collaboration between Den norske stats oljeselskap (Statoil) and the Norwegian Academy of Sciences and Letters. We thank H. H. Hardy for valuable comments. The work has received support from NFR through a grant of computer time.

[1] A. K. Singhal, J. Can. Pet. Technol. **35**, 56 (1996).
[2] M. Muskat and R. Wyckhoff, Trans. Am. Inst. Min. Metall. Pet. Eng. **114**, 144 (1935).
[3] H. I. Meyer and A. O. Garder, J. Appl. Phys. **25**, 1400 (1954).
[4] P. Chaney and M. Noble, Oil Gas J. **55**, 108 (1956).
[5] R. E. Kidder, J. Appl. Phys. **27**, 867 (1956).
[6] G. L. Chierici and G. Giucci, J. Pet. Technol. 231 (August, 1964).
[7] I. Chaperon, SPE 15377 (Soc. of Petr. Eng.) (1985).
[8] M. Wheatley, SPE 14210 (Soc. of Petr. Eng.) (1985).
[9] F. Giger, SPE 15378 (Soc. of Petr. Eng.) (1986).
[10] S. Lucas, J. Blake, and A. Kucera, J. Aust. Math. Soc. B, Appl. Math. **32**, 261 (1991); S. Lucas and A. Kucera, Phys. Fluids **8**, 3008 (1996); H. Zhang and G. C. Hocking, J. Aust. Math. Soc. B, Appl. Math. **38**, 240 (1996).
[11] A. R. Khan, J. Pet. Technol. 249 (June, 1970).
[12] N. Mungan, J. Can. Pet. Technol. **18**, 66 (1979).
[13] V. S. V. Rajan and R. W. Luhning, J. Can. Pet. Technol. **32**, 37 (1993).
[14] R. Schols, Erdoel, Erdgas **88**, 6 (1972).
[15] D. P. Sobocinski and A. J. Cornelius, J. Pet. Technol. 594 (May, 1965).
[16] E. Ozkan and R. Raghaven, SPE 20964 (Soc. of Petr. Eng.) (1990).
[17] P. Papatzacos, T. Herring, R. Martinsen, and S. Skjaeveland, SPE Reservoir Eng. **6**, 311 (1991).
[18] G. Wagner *et al.*, Phys. Rev. E **55**, 7015 (1997).
[19] A. Birovljev, Ph.D. thesis, University of Oslo, 1994.
[20] R. Lenormand and S. Bories, C.R. Acad. Sci. Paris **291**, 279 (1980).
[21] D. Wilkinson and J. F. Willemsen, J. Phys. A **16**, 3365 (1983).
[22] W. H. Press, B. P. Flannery, S. A. Teukolsky, and W. T. Vetterling, *Numerical Recipes* (Cambridge University Press, Cambridge, England, 1986).
[23] S. Ekrann, in Proceedings of the Sixth *European Symposium on Improved Oil Recovery* (STATOIL, Stavanger, 1991), Vol. 1, pp. 169–178.
[24] R. Lenormand, E. Touboul, and C. Zarcone, J. Fluid Mech. **189**, 165 (1988).
[25] D. Wilkinson, Phys. Rev. A **30**, 520 (1984).
[26] J. P. Hulin *et al.*, Phys. Rev. Lett. **61**, 333 (1988).
[27] A. Birovljev *et al.*, Phys. Rev. Lett. **67**, 584 (1991); P. Meakin, J. Feder, V. Frette, and T. Jøssang, Phys. Rev. A **46**, 3357 (1992).
[28] M. Chaouche *et al.*, Phys. Rev. E **49**, 4133 (1994).
[29] L. M. Hirsch and A. H. Thompson, Phys. Rev. E **50**, 2069 (1994).
[30] A. Vedvik *et al.*, Phys. Rev. Lett. **80**, 3065 (1998).
[31] L. Paterson, Phys. Rev. Lett. **52**, 1621 (1984).
[32] R. Lenormand, Physica A **140**, 114 (1986).
[33] V. Frette *et al.*, Phys. Rev. A **42**, 3432 (1990).